Science
AAAS

Supplementary Materials for

ApoE isoform and microbiota-dependent progression of neurodegeneration in a mouse model of tauopathy

Seo *et al.*

Correspondence to: holtzman@wustl.edu

This PDF file includes:

Figs. S1 to S18

Other Supplementary Materials for this manuscript include the following:

Table S1 [Statistical table]
Data S1 to S8 [Full gene lists]
MDAR Reproducibility Checklist

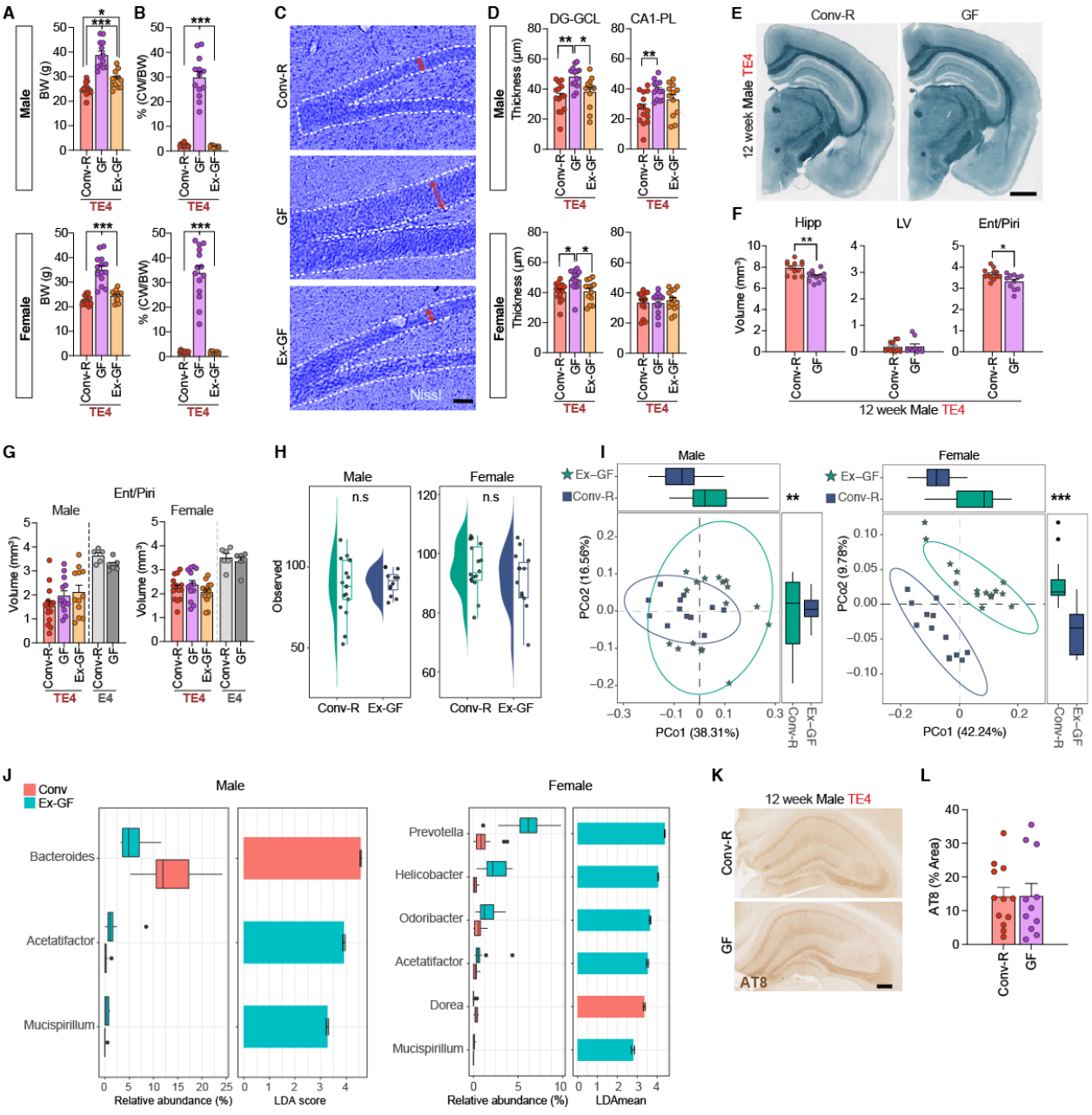

Fig. S1. Body weight, cecal weight, neuronal thickness, volume of entorhinal/piriform (Ent/Piri) cortex, and microbiota diversity comparison (related to Fig.1).

(**A,B**) Body and cecal weights at 40 weeks of age. (**C**) Representative image of granule cell layer of the dentate gyrus (DG-GCL) stained with cresyl violet. Scale bar, 30µm. (**D**) Thickness of the DG-GCL (left) and pyramidal cell layer of the CA1 region (right, CA1-PL) in male (top) and female (bottom) mice. (**E**) Representative images brain sections from 12-week-old conventionally-raised (Conv-R) and germ-free (GF) mice, stained with Sudan black. Scale bar, 1mm. (**F**) Quantification of the average volume of the hippocampus (left, Hipp), lateral ventricles (middle, LV), entorhinal/piriform cortex (right, Ent/Piri) in 12-week old TE4 animals. (**G**) Quantification of the average volume of the entorhinal/piriform (Ent/Piri) cortex in male (top) and female (bottom) mice at 40 weeks of age (related to **Fig. 1D**). (**H**) Alpha diversity (richness; observed

ASVs) in microbiota collected from 40 week-old Conv-R and Ex-GF male (left) and female (right) mice. (**I**) Beta diversity metric (weighted UniFrac) grouped by treatments (Conv-R vs. Ex-GF) in male (left) and female (right) at 40 weeks of age. (**J**) Linear Discriminant Analysis (LDA) scores for Conv-R and Ex-GF mice. Horizontal bars represent the LDA scores for each genus-level taxon in male (left) and female (right) mice. Pink and cyan bars represent taxon features with significantly higher representation in mice belonging to the Conv-R versus Ex-GF groups, respectively (LDA scores > 2). (**K**) Representative images of AT8 staining in the hippocampus from male Conv-R and GF mice at 12 weeks of age. Scale bar, 250μm. (**L**) Quantification of the percentage of area covered by AT8 staining of hippocampal sections. E4 represents human APOE4 knock-in mice in the absence of P301S tau transgene. Data are presented as mean values ± SEM (*n*=12-14/group for panels A-D and G; *n*=11-12/group for panels F,L) and statistical significance defined by one-way ANOVA with Tukey's post-hoc test for panels A-D and G, t-tests for panels F,H, and L, and PERMANOVA for panel I. n.s., not significant, *, $p < 0.05$, **, $p < 0.01$, ***, $p < 0.001$. (See **Table S1** for results of full statistical results).

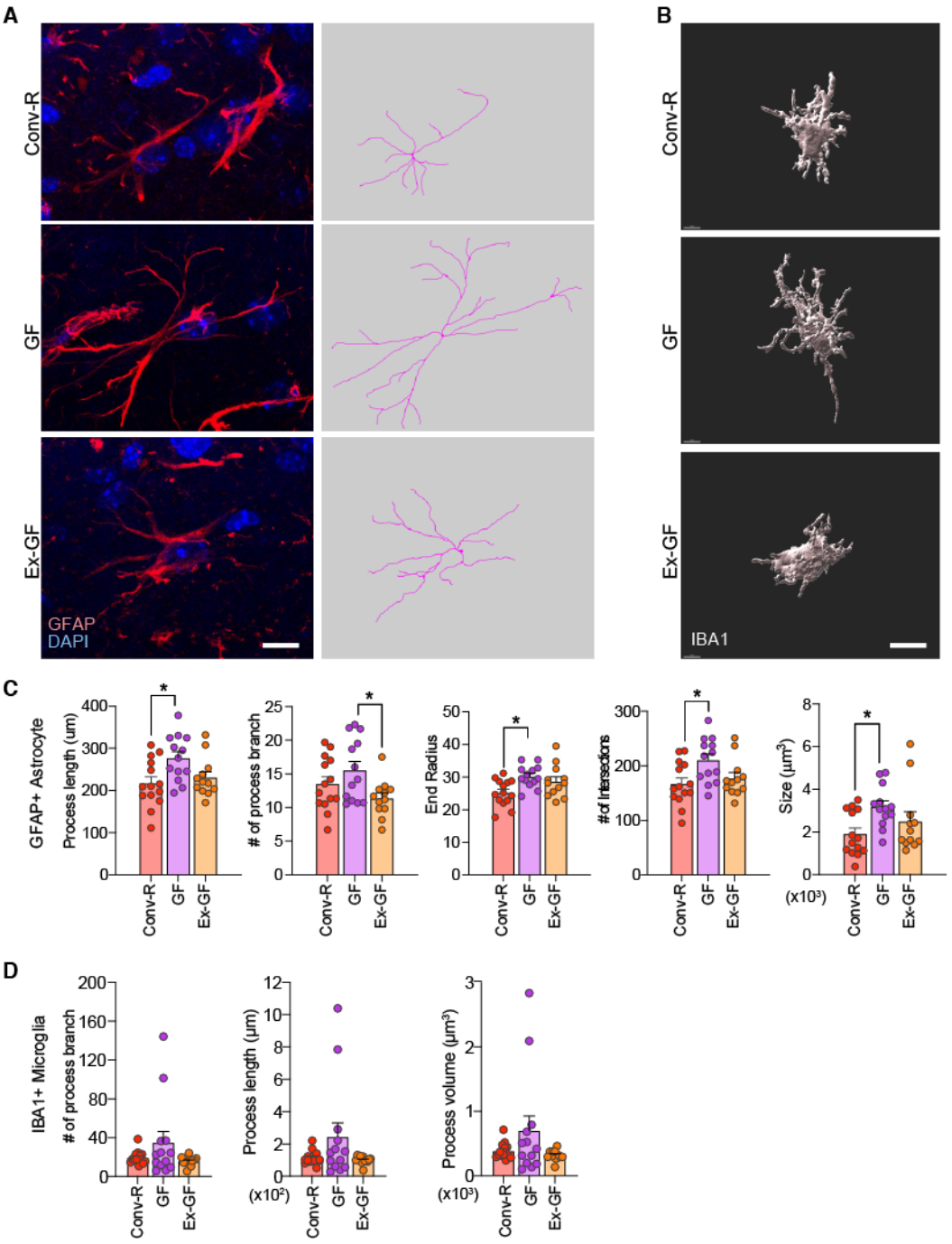

Fig. S2. Germ-free TE4 mice exhibit altered glial morphology (related to Fig.2).
(**A**) Representative high-magnification images of Conv-R, GF, Ex-GF mouse brain sections stained GFAP/DAPI (left). Representative traces of GFAP expression from Simple Neurite Tracer for each condition (right). (**B**) Representative image of Iba1+ reconstruction based on Imaris. Scale bar 10µm. (**C**) Morphometric analysis of astrocyte process length, number of process branches, end radius (based on Sholl analysis), total number of process intersections (based on Sholl analysis), and size of GFAP+ astrocytes (based on Convex Hull analysis). (**D**) Microglial morphometry data including number of branches, process length, and process volume, as

quantified by Imaris-based automatic reconstruction image of Iba1+ microglia in the dentate gyrus. Mean values ± SEM are shown. (n=12-14/group). Statistical significance was defined by one-way ANOVA with Tukey's post-hoc test. *, $p < 0.05$ (See **Table S1** for full statistical results).

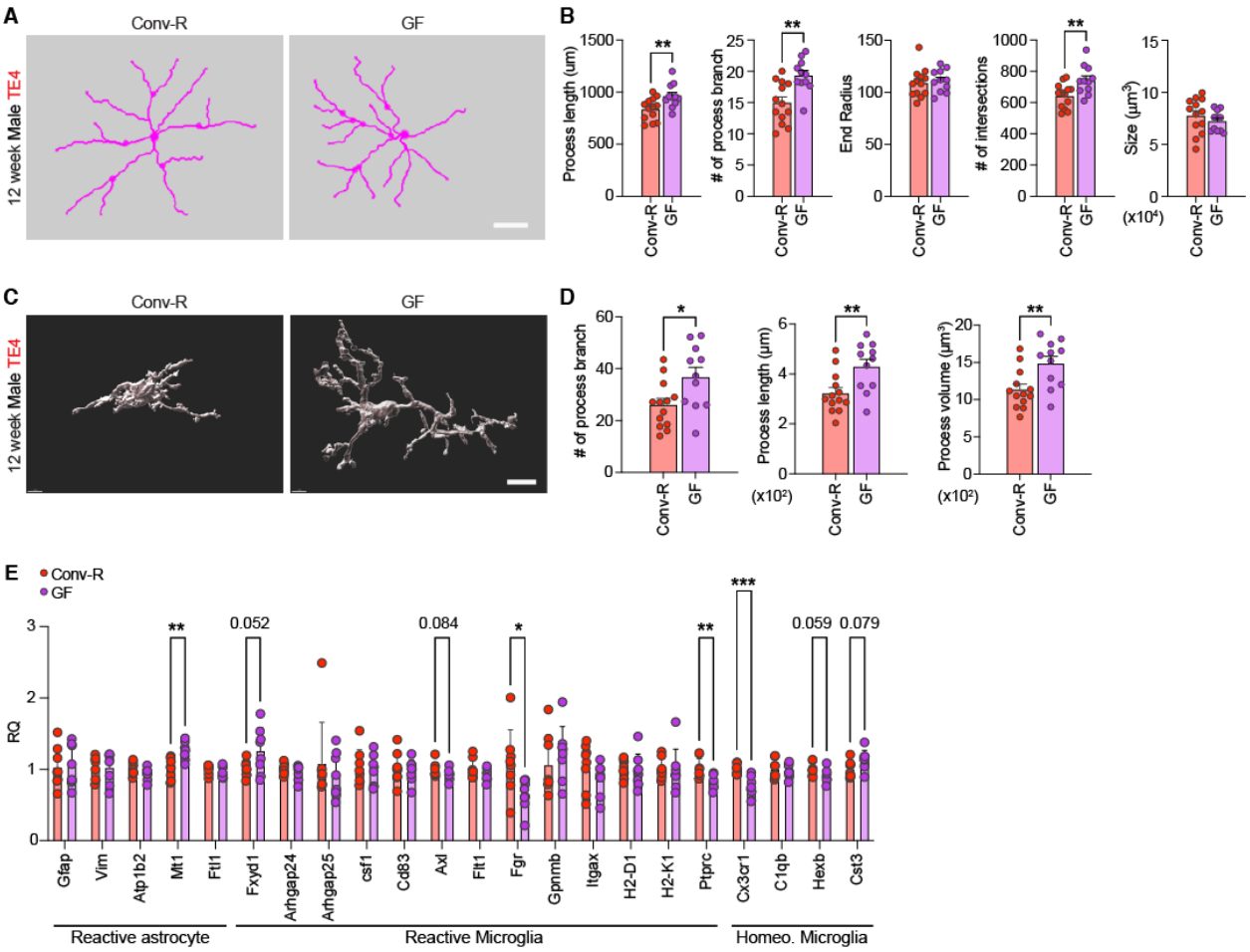

Fig. S3. Absence of microbiota altered glial morphology and gene expression at twelve weeks of age (related to Fig. S1E,F,K,L).

(**A**) Representative traces of GFAP+ astrocyte from Simple Neurite Tracer from male 12-week-old TE4 mice that were conventionally-raised (Conv-R; left) or maintained germ-free (GF; right). Scale bar 10µm. (**B**) Morphometric analysis of astrocyte process length, number of process branches, end radius (based on Sholl analysis), total number of process intersections (based on Sholl analysis), and size of GFAP+ astrocytes (based on Convex Hull analysis), in the dentate gyrus, corresponding to (A). (**C**) Representative image of Iba1+ reconstruction based on Imaris from male 12-week-old Conv-R (left) or GF (right). Scale bar 10µm. (**D**) Microglial morphometry data including number of process branches, process length, and process volume, as quantified by Imaris-based automatic reconstruction image of Iba1+ microglia in the dentate gyrus, corresponding to (C). (**E**) Glia-related gene expression was measured by qPCR using hippocampal tissues from male 12-week-old Conv-R or GF mice. Y-axis represents relative quantification of gene expression (RQ;$2^{-\Delta\Delta Ct}$) calibrating to Conv-R. Marker genes were categorized as reactive astrocyte, reactive microglia, and homeostatic microglia. The categorization of reactive astrocyte and microglia is also corresponding to the cluster 1 of glial marker genes in **Fig. 4** and **Fig. S9A,B**. Numbers above bars indicate the p-values that were close to statistical significance. Data are presented as mean values ± SEM (n=11-12/group for panels A-H; n=8/group for panel E) and statistical significance defined by t-test. *, $p < 0.05$, **, $p < 0.01$, ***, $p < 0.001$. (See **Table S1** for results of full statistical results).

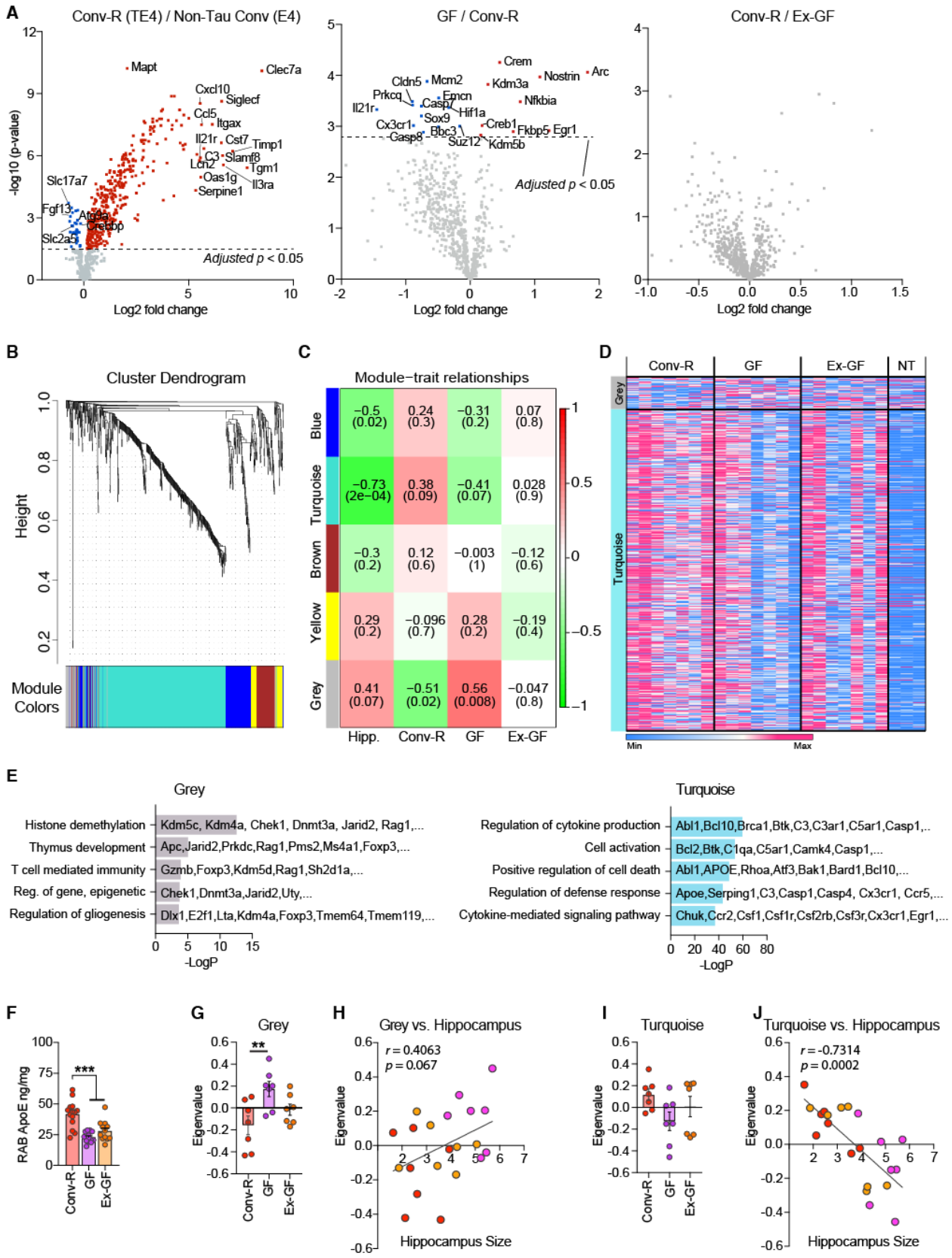
A
Conv-R (TE4) / Non-Tau Conv (E4)
GF / Conv-R
Conv-R / Ex-GF
-log10 (p-value)
Log2 fold change
Adjusted p < 0.05
Mapt
Clec7a
Cxcl10
Siglecf
Ccl5
Itgax
Il21r
Cst7
Timp1
C3
Slamf8
Lcn2
Tgm1
Oas1g
Il3ra
Serpine1
Slc17a7
Fgf13
Atp6v1a
Crebbp
Slc2a13
Crem
Nostrin
Arc
Cldn5
Mcm2
Kdm3a
Prkcq
Emcn
Nfkbia
Il21r
Casp7
Hif1a
Sox9
Cx3cr1
Creb1
Fkbp5
Egr1
Bbc3
Casp8
Suz12
Kdm5b
B
Cluster Dendrogram
Height
Module Colors
C
Module−trait relationships
Blue
Turquoise
Brown
Yellow
Grey
−0.5 (0.02)
0.24 (0.3)
−0.31 (0.2)
0.07 (0.8)
−0.73 (2e−04)
0.38 (0.09)
−0.41 (0.07)
0.028 (0.9)
−0.3 (0.2)
0.12 (0.6)
−0.003 (1)
−0.12 (0.6)
0.29 (0.2)
−0.096 (0.7)
0.28 (0.2)
−0.19 (0.4)
0.41 (0.07)
−0.51 (0.02)
0.56 (0.008)
−0.047 (0.8)
Hipp.
Conv-R
GF
Ex-GF
D
Conv-R
GF
Ex-GF
NT
Grey
Turquoise
Min
Max
E
Grey
Histone demethylation
Kdm5c, Kdm4a, Chek1, Dnmt3a, Jarid2, Rag1,...
Thymus development
Apc,Jarid2,Prkdc,Rag1,Pms2,Ms4a1,Foxp3,...
T cell mediated immunity
Gzmb,Foxp3,Kdm5d,Rag1,Sh2d1a,...
Reg. of gene, epigenetic
Chek1,Dnmt3a,Jarid2,Uty,...
Regulation of gliogenesis
Dlx1,E2f1,Lta,Kdm4a,Foxp3,Tmem64,Tmem119,...
-LogP
Turquoise
Regulation of cytokine production
Abl1,Bcl10,Brca1,Btk,C3,C3ar1,C5ar1,Casp1,..
Cell activation
Bcl2,Btk,C1qa,C5ar1,Camk4,Casp1,...
Positive regulation of cell death
Abl1,APOE,Rhoa,Atf3,Bak1,Bard1,Bcl10,...
Regulation of defense response
Apoe,Serping1,C3,Casp1,Casp4, Cx3cr1, Ccr5,...
Cytokine-mediated signaling pathway
Chuk,Ccr2,Csf1,Csf1r,Csf2rb,Csf3r,Cx3cr1,Egr1,...
-LogP
F
RAB ApoE ng/mg
Conv-R
GF
Ex-GF
G
Grey
Eigenvalue
H
Grey vs. Hippocampus
r = 0.4063
p = 0.067
Eigenvalue
Hippocampus Size
I
Turquoise
Eigenvalue
J
Turquoise vs. Hippocampus
r = -0.7314
p = 0.0002
Eigenvalue
Hippocampus Size

Fig. S4. Absence of the microbiota impacts the glial transcriptomic profile (related to Fig.1). (**A**) Volcano plot showing statistical significance (P_{adj}) vs. fold-difference for genes differentially expressed as a result of (i) the presence versus absence of the tau transgene (left; Conv-R:TE4 versus Conv-R E4; see Data S1 for full gene list), germ-free versus conventionally-raised state (middle; GF versus Conv-R; see Data S2 for full gene list), and colonization of formerly germ-free animals (right; Conv-R versus Ex-GF; Data S3 for full gene list) (n=7 for Conv-R, GF, and Ex-GF. n=3 for Non-Tau). Red and blue symbols denote up-regulated and down-regulated genes respectively with adjusted significance of $p < 0.01$. (**B**) WGCNA dendrogram group genes measured in the hippocampus of Conv-R, GF and Ex-GF mice into distinct modules, defined by dendrogram branch clustering. (**C**) Module-trait analysis between gene modules defined by WGCNA and housing conditions or hippocampus size (Hipp). Data are shown as correlation coefficients (p value). (**D**) Heatmap of relative expression of Turquoise and Grey module genes. (**E**) Gene Ontology (GO) Biological Process terms associated with Grey (left) and Turquoise (right) modules, ranked by p-value with top 5 processes listed. (**F**) Total human APOE concentration measured by ELISA in RAB fraction from the cortex of 40-week-old mice (n=12-14/group) (**G**) Eigengene analysis for Grey module by GF vs. Conv-R conditions. (**H**) Correlation analysis between hippocampal size and Grey module eigenvalue of each individual. (**I**) Eigengene analysis for Turquoise module by GF vs. Conv-R conditions. (**J**) Correlation analysis between hippocampal size and Turquois module eigenvalue of each individual mouse. Statistical significance was defined by one-way ANOVA with Tukey's post-hoc test. **, $p < 0.01$, ***, $p < 0.001$. (See **Table S1** for full statistical results and **Data S1-S4** for the full list of genes).

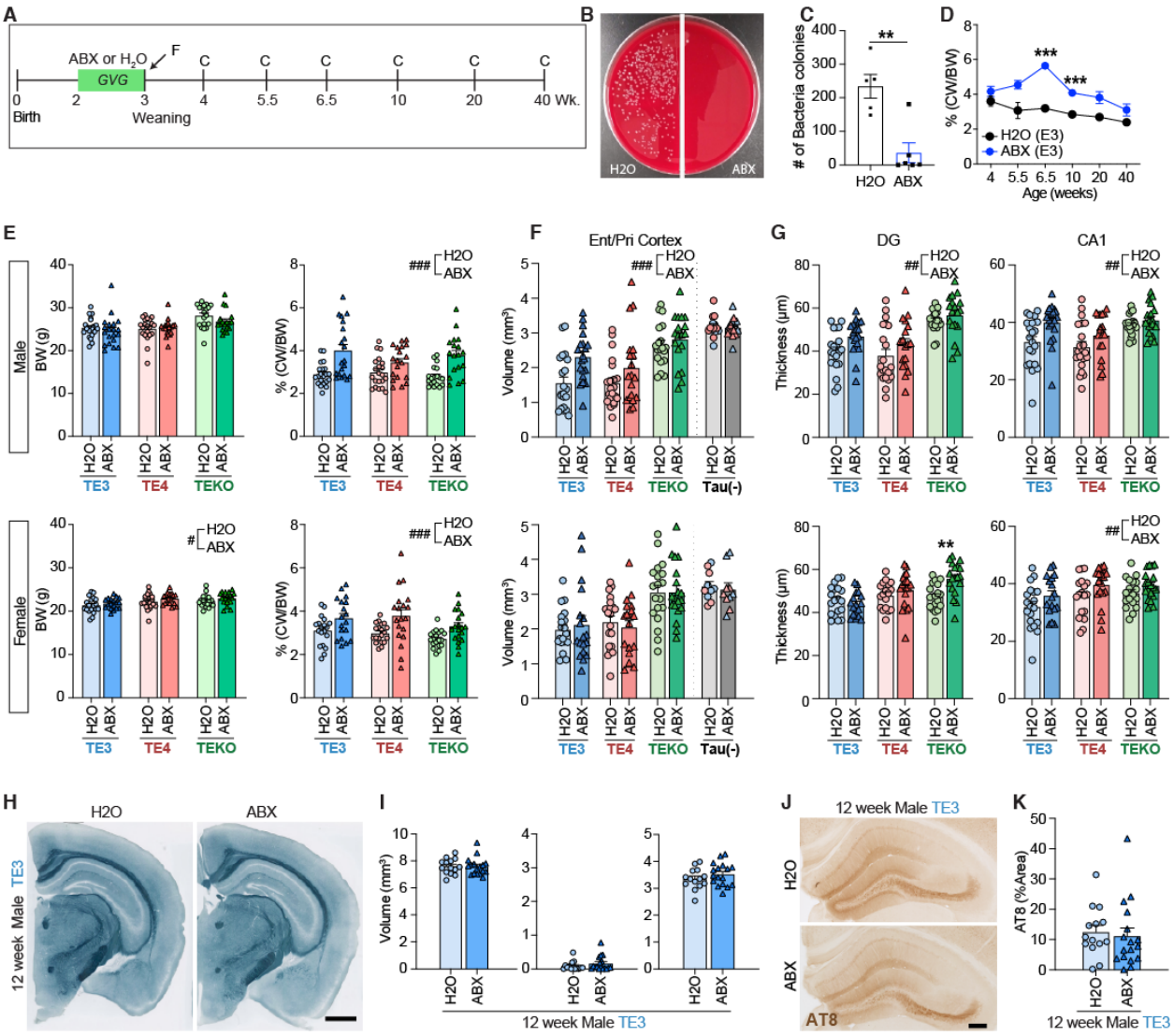

Fig. S5. Monitoring the effect of ABX treatment on gut bacterial viability, body weight, cecal weight, neuronal thickness, volume of Ent/Piri cortex (related to Fig. 3).

(A) Experimental scheme. (**B,C**) Reduction in viable fecal bacteria after seven days of ABX treatment of E3 mice. Panel B shows results obtained after 24 h growth on Brucella medium. (**D**) Quantification of the cecal weights on different time points after treatment with H2O/ABX. (**E**) Body weights (left) and cecal weights (right) in male (top) and female (bottom) mice at 40 weeks of age, related to **Fig. 3** (n=18-21 mice/group). (**F**) Quantification of the average volume of the entorhinal/piriform (Ent/Piri) cortex in male (top) and female (bottom) mice, related to **Fig. 3C**. Tau (-) represents APOE3 (blue) or APOE4 (red) knock-in mice that lack the P301S tau transgene. (**G**) Thickness of the granule cell layer of the dentate gyrus (left; DG-GCL) and pyramidal cell layer of the CA1 (right, CA1-PL) in 40-week-old male (top) and female (bottom) mice. (**H**) Representative images of brain sections, stained with Sudan black, from 12-week-old male TE3 mice treated with H2O/ABX. Scale bar, 1mm. (**I**) Quantification of the volumes of the hippocampus (left, Hipp), lateral ventricles (middle, LV), entorhinal/piriform cortex (right, Ent/Piri) (*n*=14-17/group) (**J**) Representative images of AT8 staining in the hippocampus from 12-week-old male TE3 mice treated with ABX or H20. Scale bar, 250µm. (**K**) Percentage of area

covered by AT8 staining in the hippocampus. Data are presented as mean values ± SEM. Statistical significance was tested with two-way ANOVA with Tukey's post-hoc test for panels D-G and t-test for panels C,I and K. **, $p < 0.01$, ***, $p < 0.001$. Statistical significances of the main effects of treatments (H2O vs. ABX) were indicated as #, $p < 0.05$, ##, $p < 0.01$, ###, $p < 0.001$. (See **Table S1** for full statistical results).

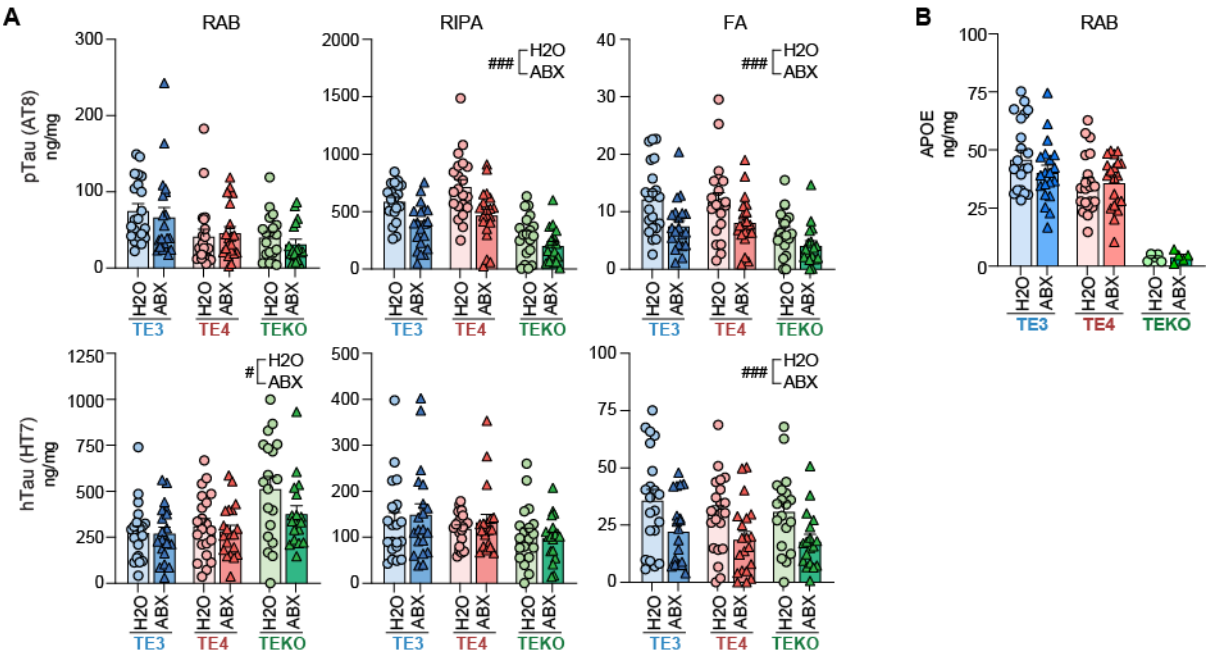

Fig. S6. ABX treatment is associated with reduced levels of detergent soluble and insoluble p-Tau, and insoluble human Tau, but with not soluble ApoE.
(**A**) Concentrations of p-tau and human total tau in RAB, RIPA, and FA fractions, respectively, from the cerebral cortex. (**B**) Total human APOE concentration in RAB fraction from the cortex. Data are presented as mean values ± SEM (*n*=18-21/group). Statistical significance was defined by two-way ANOVA. The main effects of treatments (H2O vs. ABX) were indicated as #, $p < 0.05$, ###, $p < 0.001$. (See **Table S1** for full statistical results).

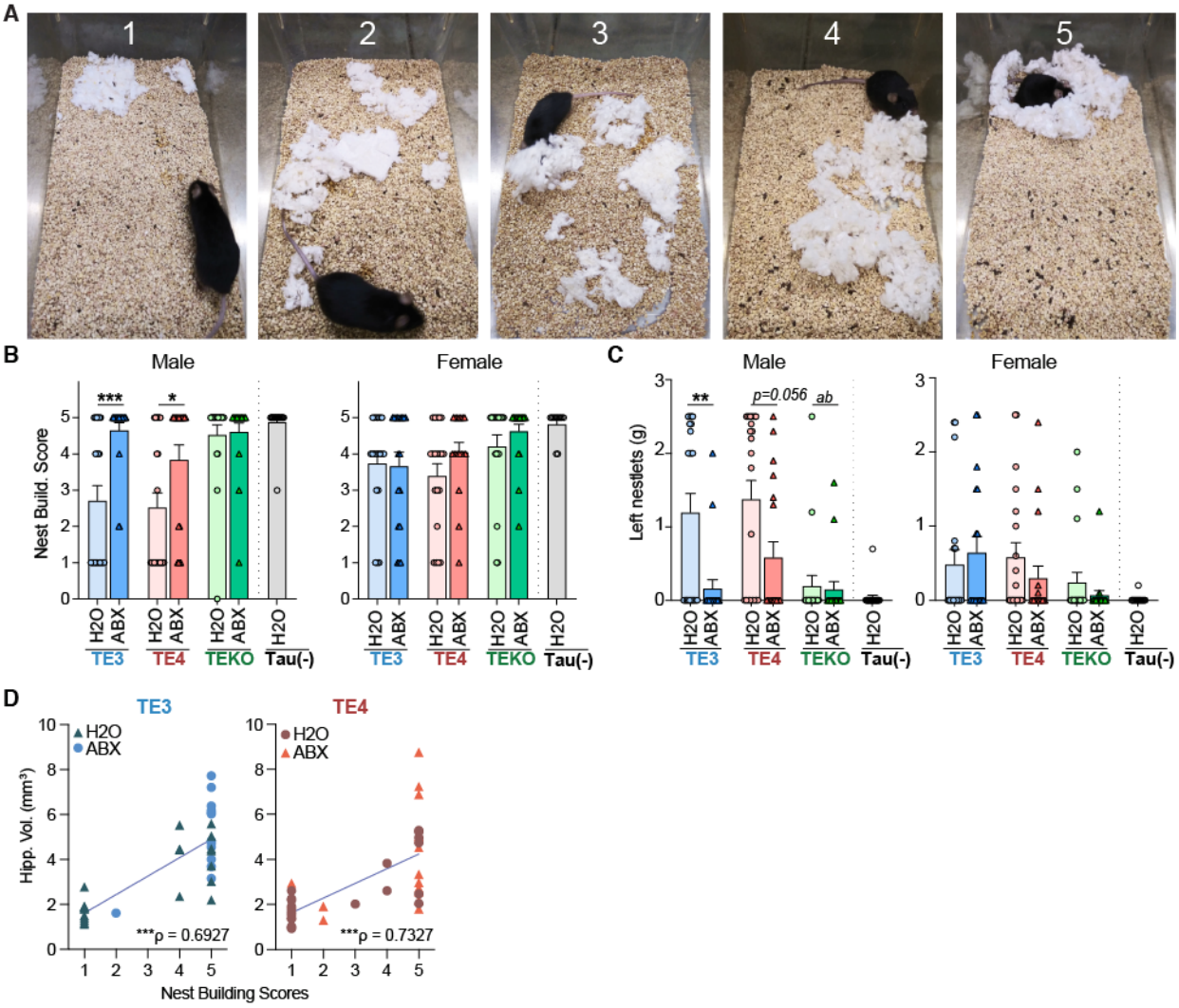

Fig. S7. ABX treatment protects against impaired nest building behavior.
Nest building behavior testing was performed 3-4 days before euthanizing animals that were 40 weeks of age. (**A**) Representative images of nests built by each mouse and the corresponding score: no nest, 1, to completed nest, 5. (**B**) Quantification of the nest building test scores. Fisher's exact test was to define the statistical significance of differences observed between treatments. (**C**) The remaining nestlets were weighed for each mouse and averaged per treatment group. Statistical significance defined by two-way ANOVA with Tukey's post-hoc test. (**D**) Correlation plot between hippocampal volume (Hipp. Vol.) and nest building scores. All data are expressed as mean values ± SEM (n=18-21/group). *, $p < 0.05$, **, $p < 0.01$, ***, $p < 0.001$. '*ab*' in panel C indicates statistical significance compared to TE3-H2O and TE4-H2O groups, respectively ($p < 0.001$). (See **Table S1** for full statistical results).

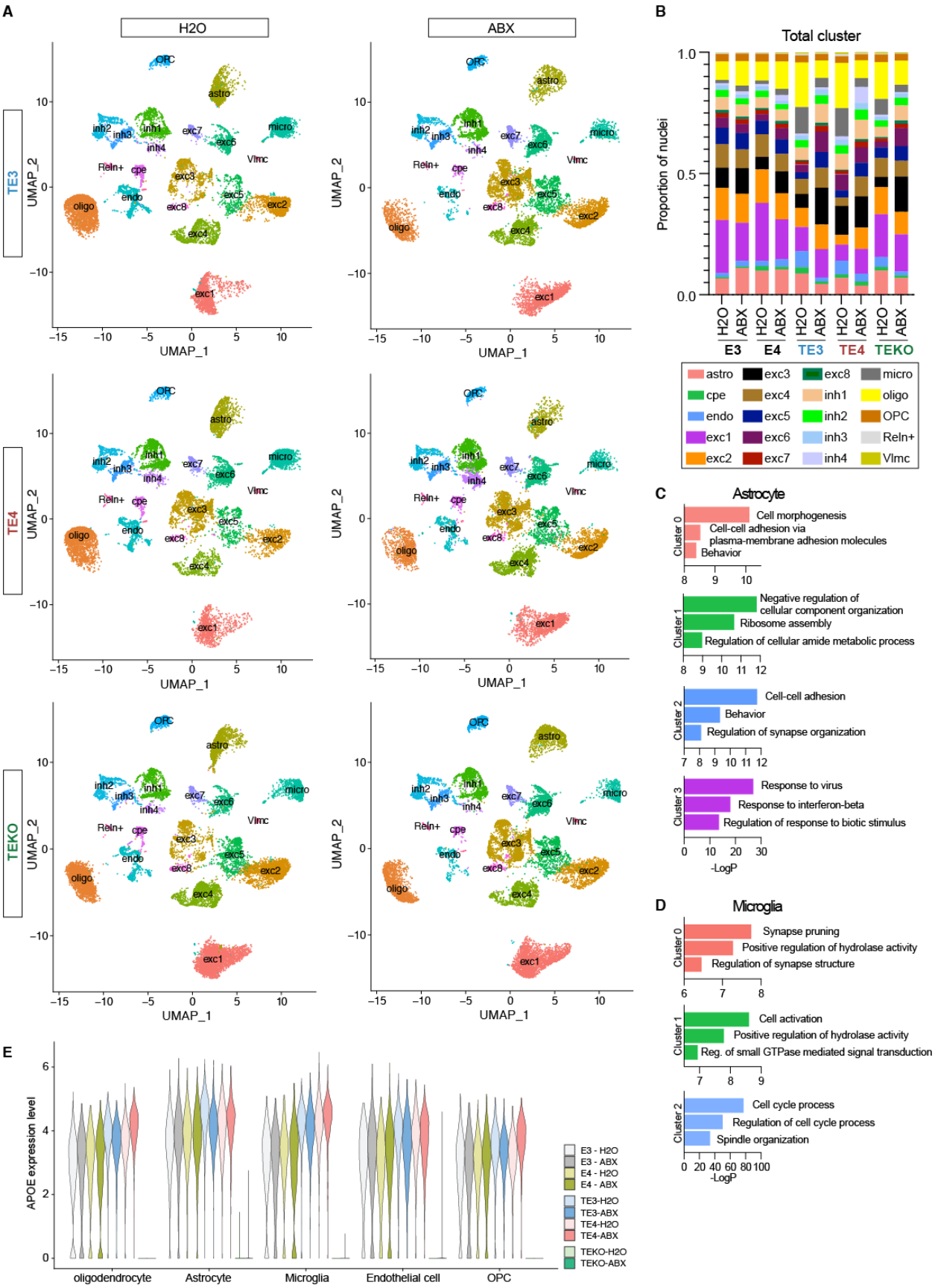
A
H2O
ABX
TE3
TE4
TEKO
UMAP_1
UMAP_2
ORC
astro
inh1
inh2
inh3
inh4
exc1
exc2
exc3
exc4
exc5
exc6
exc7
exc8
micro
Vlmc
Reln+
cpe
endo
oligo
B
Total cluster
Proportion of nuclei
H2O
ABX
E3
E4
TE3
TE4
TEKO
astro
cpe
endo
exc1
exc2
exc3
exc4
exc5
exc6
exc7
exc8
inh1
inh2
inh3
inh4
micro
oligo
OPC
Reln+
Vlmc
C
Astrocyte
Cluster 0
Cell morphogenesis
Cell-cell adhesion via plasma-membrane adhesion molecules
Behavior
Cluster 1
Negative regulation of cellular component organization
Ribosome assembly
Regulation of cellular amide metabolic process
Cluster 2
Cell-cell adhesion
Behavior
Regulation of synapse organization
Cluster 3
Response to virus
Response to interferon-beta
Regulation of response to biotic stimulus
-LogP
D
Microglia
Cluster 0
Synapse pruning
Positive regulation of hydrolase activity
Regulation of synapse structure
Cluster 1
Cell activation
Positive regulation of hydrolase activity
Reg. of small GTPase mediated signal transduction
Cluster 2
Cell cycle process
Regulation of cell cycle process
Spindle organization
-LogP
E
APOE expression level
oligodendrocyte
Astrocyte
Microglia
Endothelial cell
OPC
E3 - H2O
E3 - ABX
E4 - H2O
E4 - ABX
TE3-H2O
TE3-ABX
TE4-H2O
TE4-ABX
TEKO-H2O
TEKO-ABX

Fig. S8. snRNA-seq reveals cell type-specific transcriptional responses associated with antibiotic-induced gut microbiota perturbations, related to Fig. 3.
(**A**) Uniform manifold approximation and projection (UMAP) plot for all cell populations split by experimental groups. UMAP plot showing 20 distinguishable clusters, with corresponding cell types identified by using known cell markers. Abbreviations: Exc, excitatory neuron; Inh, inhibitory neuron; Astro, astrocyte; Micro, microglia; Oligo, oligodendrocyte; OPC, oligodendrocyte progenitor cells; cpe, choroid plexus epithelial cell; Reln+, reelin+; Vlmc, vascular and leptomeningeal cell. (**B**) Relative frequency of cell clusters in each experimental group. (**C**) GO Biological Process terms associated with each module, related to **Fig. 3A**, ranked by *p*-value ($\log_{10}$P) with top 3 GO biological processes listed. (**D**) GO terms associated with each module in **Fig. 3H**, ranked by *p*-value ($\log_{10}$P) with top 3 GO biological processes listed. (See **Data S5,6** for a complete list of genes). (**E**) APOE gene expression levels by cell-type. The y-axis represents the normalized, natural log-transformed APOE gene count. OPC, oligodendrocyte progenitor cells.

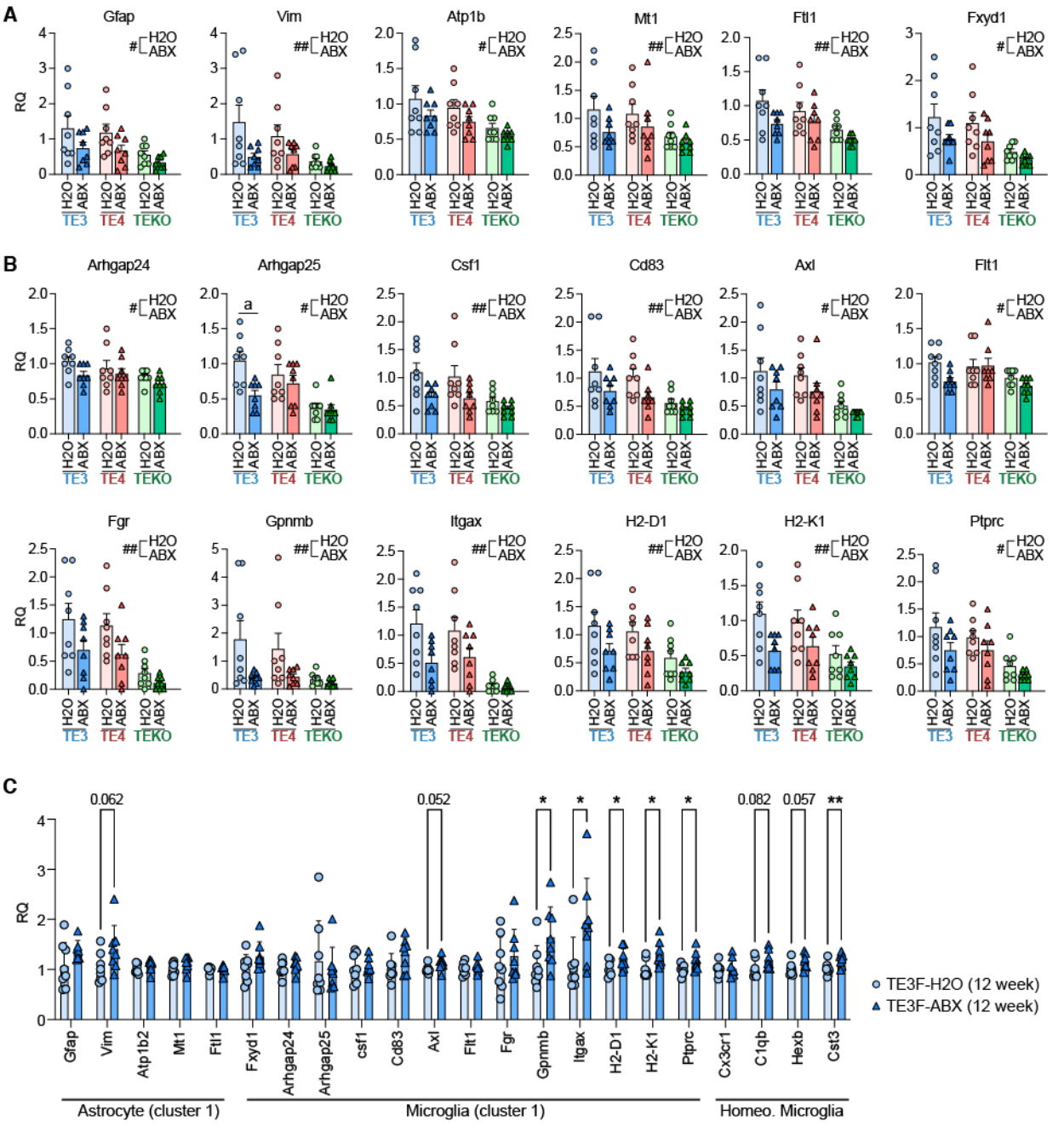

Fig. S9. ABX treatment altered glial gene expression. Validation of sn-RNA seq results, related to Fig. 3.

(**A**) Marker genes from astrocyte cluster 1 verified by qPCR using hippocampal tissue recovered from male mice (*n*=8/group) (related to **Fig. 4A,B**). Y-axis represents the relative quantification of gene expression (RQ;$2^{-\Delta\Delta Ct}$) calibrated to TE3-H2O. (**B**) Marker genes from microglia cluster 1 verified by qPCR using hippocampal tissues harvested from male mice (*n*=8/group) (related to **Fig. 4H,I**). (**C**) The marker genes were also measured using hippocampal tissue obtained from male 12-week-TE3 mice (*n*=8/group). Numbers above bars indicate p-values that were close to statistical significance. Data are presented as mean values ± SEM; Statistical significance determined by two-way ANOVA with Tukey's post-hoc test for panels A and B and t-test for panel

C. *, $p < 0.05$, **, $p < 0.01$. Statistical significances of the main effects of treatments (H2O vs. ABX) were indicated as #, $p < 0.05$, ##, $p < 0.01$, ###, $p < 0.001$. Note that '*a'* indicates that the interaction of genotype x treatment was close to significant ($p = 0.053$). (see **Table S1** for full statistical results).

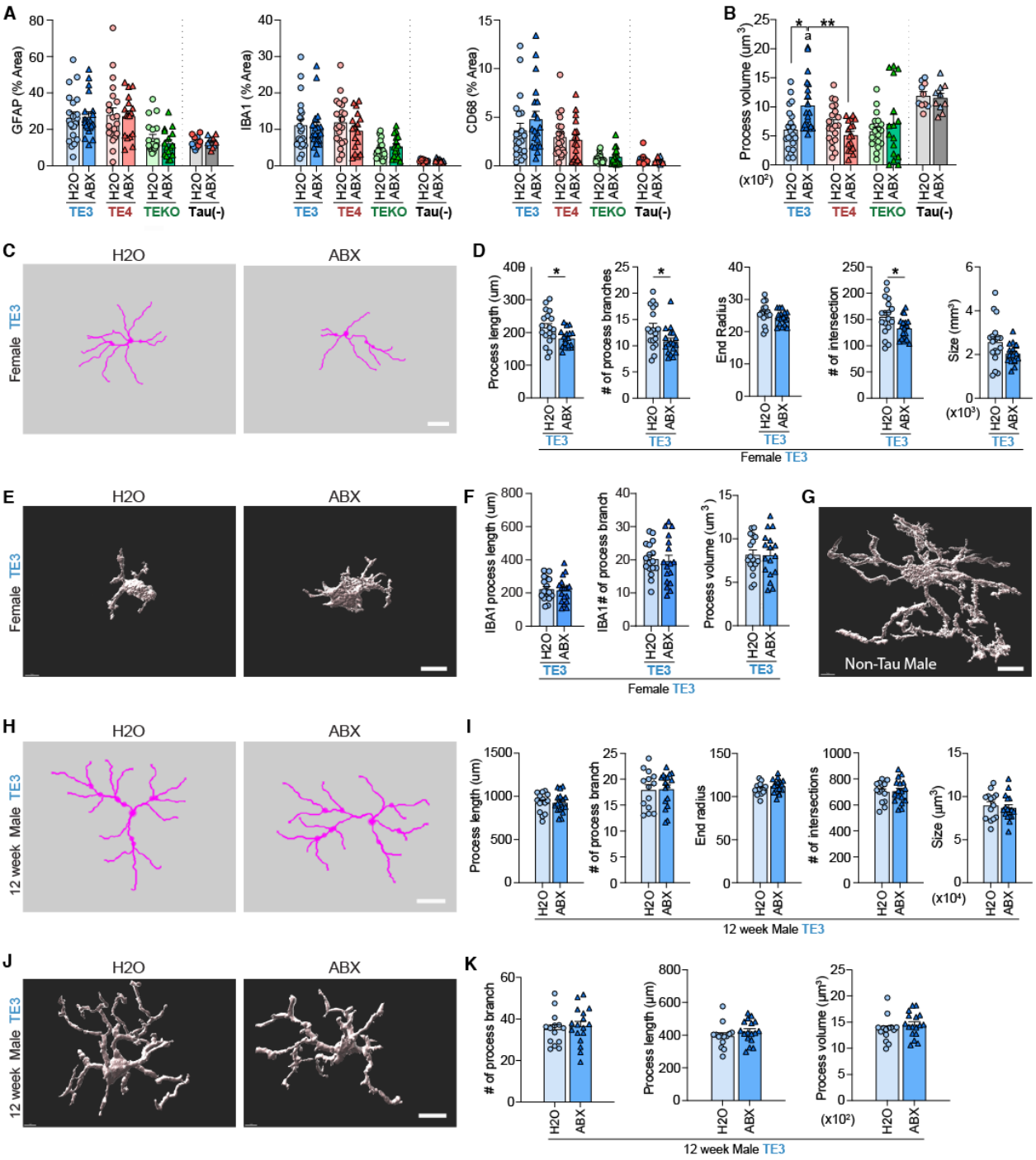

Fig. S10. ABX treatment modulates differential glial responses in a sex and ApoE isoform dependent manner, related to Fig. 3.

(**A**) Percentage of area in sections of hippocampus of male 40-week-old TE3, TE4, and TEKO mice covered by GFAP (left), Iba-1 (middle), CD68 (right) staining. (**B**) Process volume for male TE3, TE4, and TEKO mice (related to **Fig. 3J**). (**C**) Representative traces of GFAP+ astrocytes from Simple Neurite Tracer from 40-week-old female TE3 mice treated with H2O (left) or ABX (right). (**D**) Morphometry data of astrocyte process lengths, the number of branches, the end radius,

and total number of process intersections from Sholl analysis. The size of GFAP+ astrocytes, defined by Convex Hull analysis in 40-week-old female TE3 mice. (**E**) Imaris microglia reconstruction image of conventionally-raised 40-week-old female TE3 mice treated with H2O (left) or ABX (right). (**F**) Morphometry data of process length (left), number of branches (middle), process volume of Iba1+ microglial cells from 40-week-old female TE3 mice. (**G**) Imaris-based automatic reconstruction image of Iba1+ microglia in the hippocampus of a 40-week-old male mouse lacking the tau transgene (related to **Fig. 3J-L**). (**H**) Representative traces of GFAP+ astrocyte from Simple Neurite Tracer from male 12-week-old male TE3 mice treated with H2O (left) or ABX (right). (**I**) Morphometry data of astrocyte process lengths, the number of branches, the end radius, and total number of process intersections from Sholl analysis. The size of GFAP+ astrocytes, defined by Convex Hull analysis in male 12-week-old male TE3 mice. (**J**) Imaris microglia reconstruction image of male 12-week-old male TE3 mice treated with H2O (left) or ABX (right). (**K**) Morphometry data of process length (left), number of branches (middle), process volume of Iba1+ microglial cells from male 12-week-old male TE3 mice. Data are presented as mean values ± SEM; Statistical significance determined by two-way ANOVA with Tukey's post hoc for panel A-B and t-test for panel D-K. *, $p < 0.05$, **, $p < 0.01$. Statistical significance values of the main effects of treatments (H2O vs. ABX) were indicated as #, $p < 0.05$, ##, $p < 0.01$, ###, $p < 0.001$. Note that '*a'* (in panel B) indicates statistical significance compared to TEKO-H2O and TEKO-ABX animals ($p < 0.05$). (see **Table S1** for full statistical results)

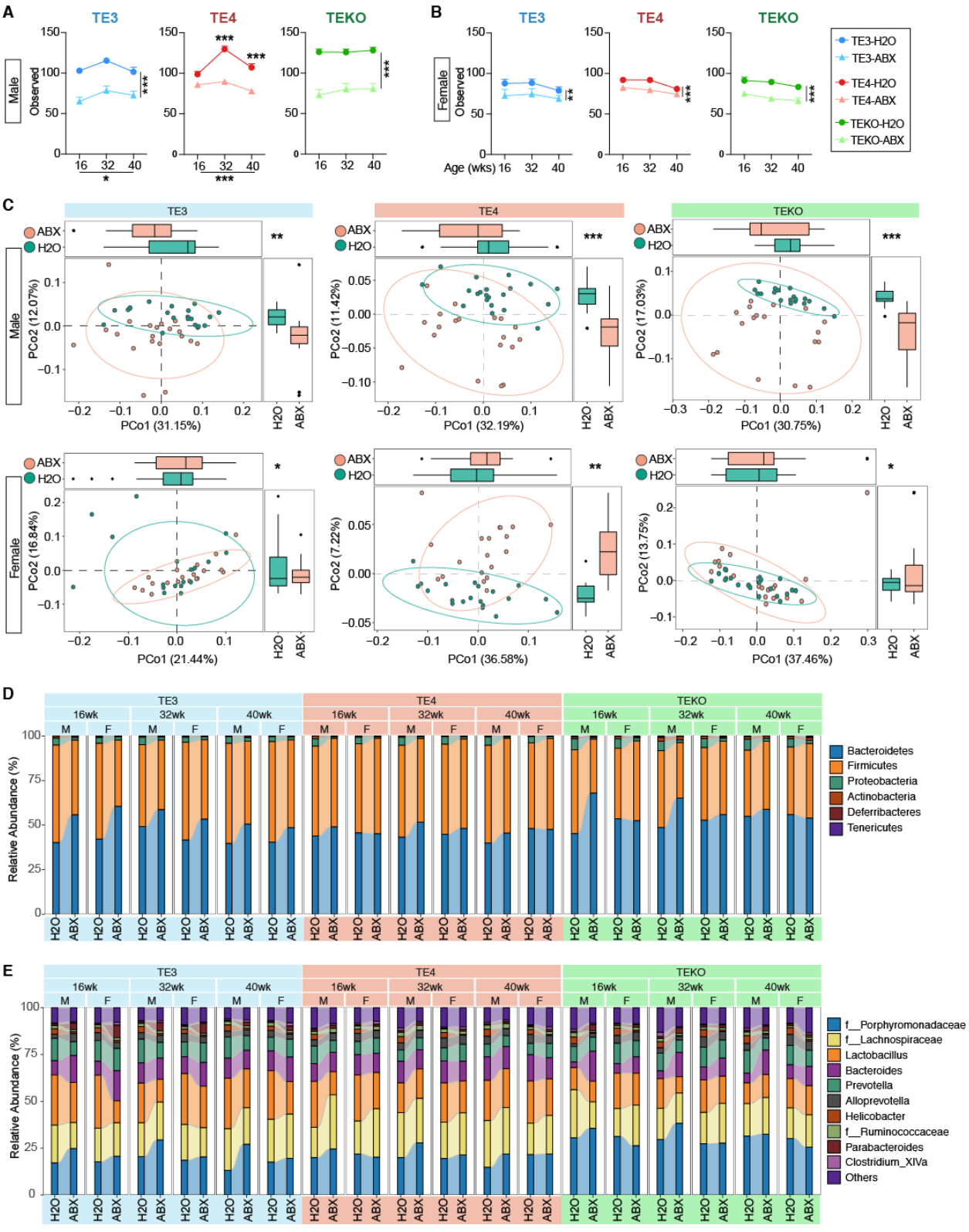

Fig. S11. Composition of the gut microbiota is altered in ABX-treated mice.
(**A,B**) Alpha diversity metric (richness; observed ASVs) over time in male (A) and female (B) TE3, TE4, and TEKO mice after being treated with H2O or ABX from postnatal days 16 to 22.

Restricted Maximum Likelihood (REML). (**C**) Beta diversity metric (weighted UniFrac) grouped by treatments (H2O vs. ABX) in male (top) and female (bottom) TE3 (left), TE4 (middle), and TEKO (right) mice. PERMANOVA at 40 weeks of age. (**D**) Phylum-level analysis of fecal microbiota composition as a function of treatments (H2O Vs. ABX) in male and female TE3, TE4, and TEKO mice over time (16, 32, 40 weeks of age). (**E**) Genera represented in the fecal microbiota in ABX or H2O-treated male and female TE3, TE4, and TEKO mice sampled at 16, 32, 40 weeks of age. Data are presented as mean values ± SEM; **, $p < 0.01$, ***, $p < 0.001$. (See **Table S1** for full statistical results).

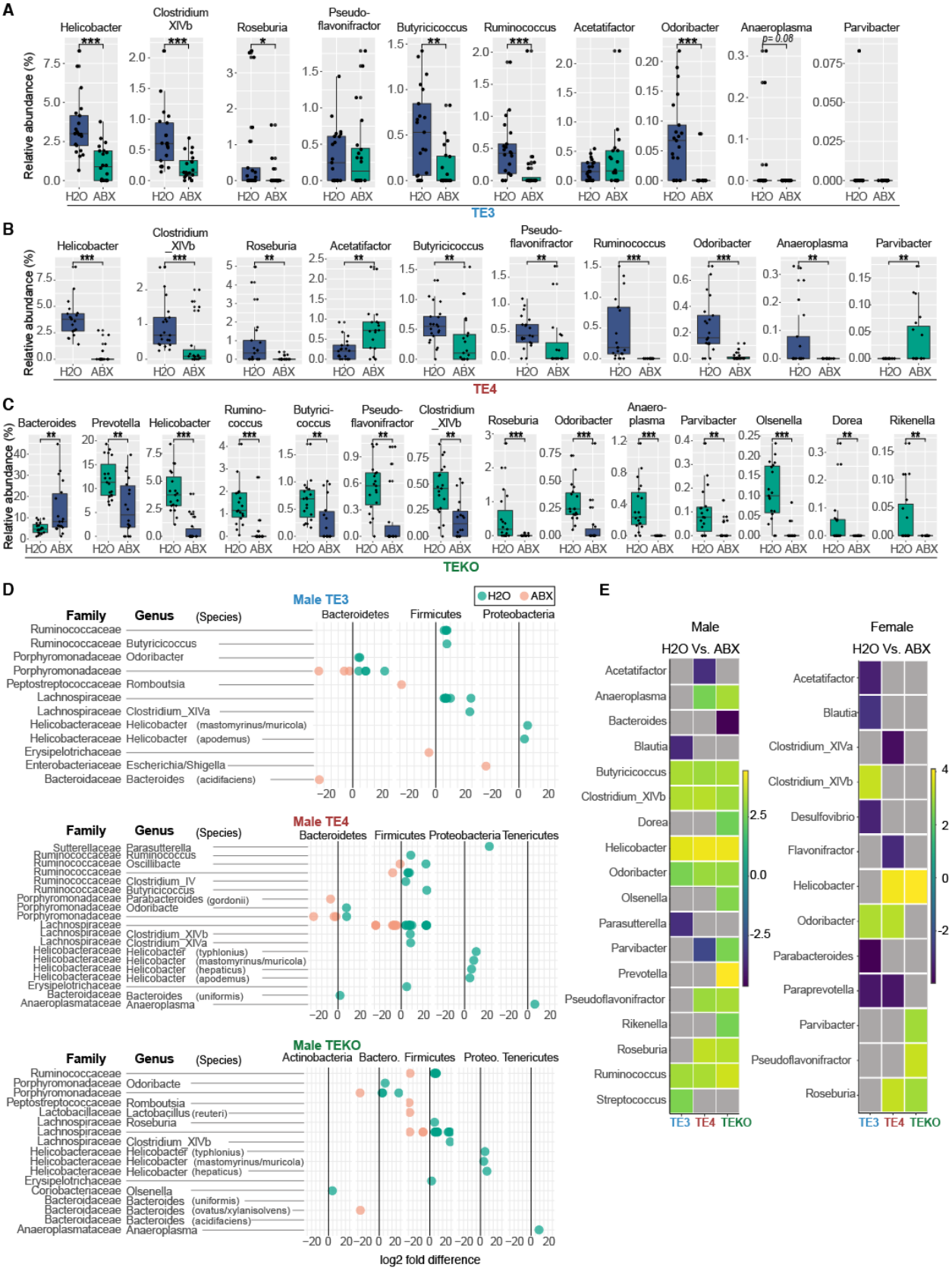
A
Helicobacter
Clostridium XlVb
Roseburia
Pseudo-flavonifractor
Butyricicoccus
Ruminococcus
Acetatifactor
Odoribacter
Anaeroplasma
Parvibacter
p= 0.08
Relative abundance (%)
H2O ABX
TE3
B
Helicobacter
Clostridium _XlVb
Roseburia
Acetatifactor
Butyricicoccus
Pseudo-flavonifractor
Ruminococcus
Odoribacter
Anaeroplasma
Parvibacter
Relative abundance (%)
H2O ABX
TE4
C
Bacteroides
Prevotella
Helicobacter
Rumino-coccus
Butyrici-coccus
Pseudo-flavonifractor
Clostridium _XlVb
Roseburia
Odoribacter
Anaero-plasma
Parvibacter
Olsenella
Dorea
Rikenella
Relative abundance (%)
H2O ABX
TEKO
D
Male TE3
H2O ABX
Family Genus (Species)
Bacteroidetes Firmicutes Proteobacteria
Ruminococcaceae
Ruminococcaceae Butyricicoccus
Porphyromonadaceae Odoribacter
Porphyromonadaceae
Peptostreptococcaceae Romboutsia
Lachnospiraceae
Lachnospiraceae Clostridium_XlVa
Helicobacteraceae Helicobacter (mastomyrinus/muricola)
Helicobacteraceae Helicobacter (apodemus)
Erysipelotrichaceae
Enterobacteriaceae Escherichia/Shigella
Bacteroidaceae Bacteroides (acidifaciens)
−20 0 20
Male TE4
Family Genus (Species)
Bacteroidetes Firmicutes Proteobacteria Tenericutes
Sutterellaceae Parasutterella
Ruminococcaceae Ruminococcus
Ruminococcaceae Oscillibacte
Ruminococcaceae
Ruminococcaceae Clostridium_IV
Ruminococcaceae Butyricicoccus
Porphyromonadaceae Parabacteroides (gordonii)
Porphyromonadaceae Odoribacte
Porphyromonadaceae
Lachnospiraceae
Lachnospiraceae Clostridium_XlVb
Lachnospiraceae Clostridium_XlVa
Helicobacteraceae Helicobacter (typhlonius)
Helicobacteraceae Helicobacter (mastomyrinus/muricola)
Helicobacteraceae Helicobacter (hepaticus)
Helicobacteraceae Helicobacter (apodemus)
Erysipelotrichaceae
Bacteroidaceae Bacteroides (uniformis)
Anaeroplasmataceae Anaeroplasma
−20 0 20
Male TEKO
Family Genus (Species)
Actinobacteria Bactero. Firmicutes Proteo. Tenericutes
Ruminococcaceae
Porphyromonadaceae Odoribacte
Porphyromonadaceae
Peptostreptococcaceae Romboutsia
Lactobacillaceae Lactobacillus (reuteri)
Lachnospiraceae Roseburia
Lachnospiraceae
Lachnospiraceae Clostridium_XlVb
Helicobacteraceae Helicobacter (typhlonius)
Helicobacteraceae Helicobacter (mastomyrinus/muricola)
Helicobacteraceae Helicobacter (hepaticus)
Erysipelotrichaceae
Coriobacteriaceae Olsenella
Bacteroidaceae Bacteroides (uniformis)
Bacteroidaceae Bacteroides (ovatus/xylanisolvens)
Bacteroidaceae Bacteroides (acidifaciens)
Anaeroplasmataceae Anaeroplasma
−20 0 20
log2 fold difference
E
Male
H2O Vs. ABX
Acetatifactor
Anaeroplasma
Bacteroides
Blautia
Butyricicoccus
Clostridium_XlVb
Dorea
Helicobacter
Odoribacter
Olsenella
Parasutterella
Parvibacter
Prevotella
Pseudoflavonifractor
Rikenella
Roseburia
Ruminococcus
Streptococcus
2.5
0.0
-2.5
TE3 TE4 TEKO
Female
H2O Vs. ABX
Acetatifactor
Blautia
Clostridium_XlVa
Clostridium_XlVb
Desulfovibrio
Flavonifractor
Helicobacter
Odoribacter
Parabacteroides
Paraprevotella
Parvibacter
Pseudoflavonifractor
Roseburia
4
2
0
-2
TE3 TE4 TEKO

Fig. S12. ABX reshapes the bacterial composition of microbial communities.
(**A-C**) Relative abundance of bacterial genera in the fecal microbiota of TE3 (A), TE4 (B), TEKO (C) mice, selected from **Fig. 5A** based on LDA scores. Statistical significance defined by t-test. (**D**) Comparison of relative abundance of taxa between treatments (H2O vs. ABX) in male 40-week-old TE3 (top), TE4 (middle), and TEKO (bottom) animals. Data are related to **Fig. 5A** and represented by log_2-fold differences. (**E**) Heatmap summarizing the relative abundances of genera, based on LDA scores comparing control H2O versus ABX in each APOE isoform, related to **Fig. 5A,B**. The color scale represents LDA score. Gray color indicates that there was not a significant difference in LDA (LDA scores < 2).

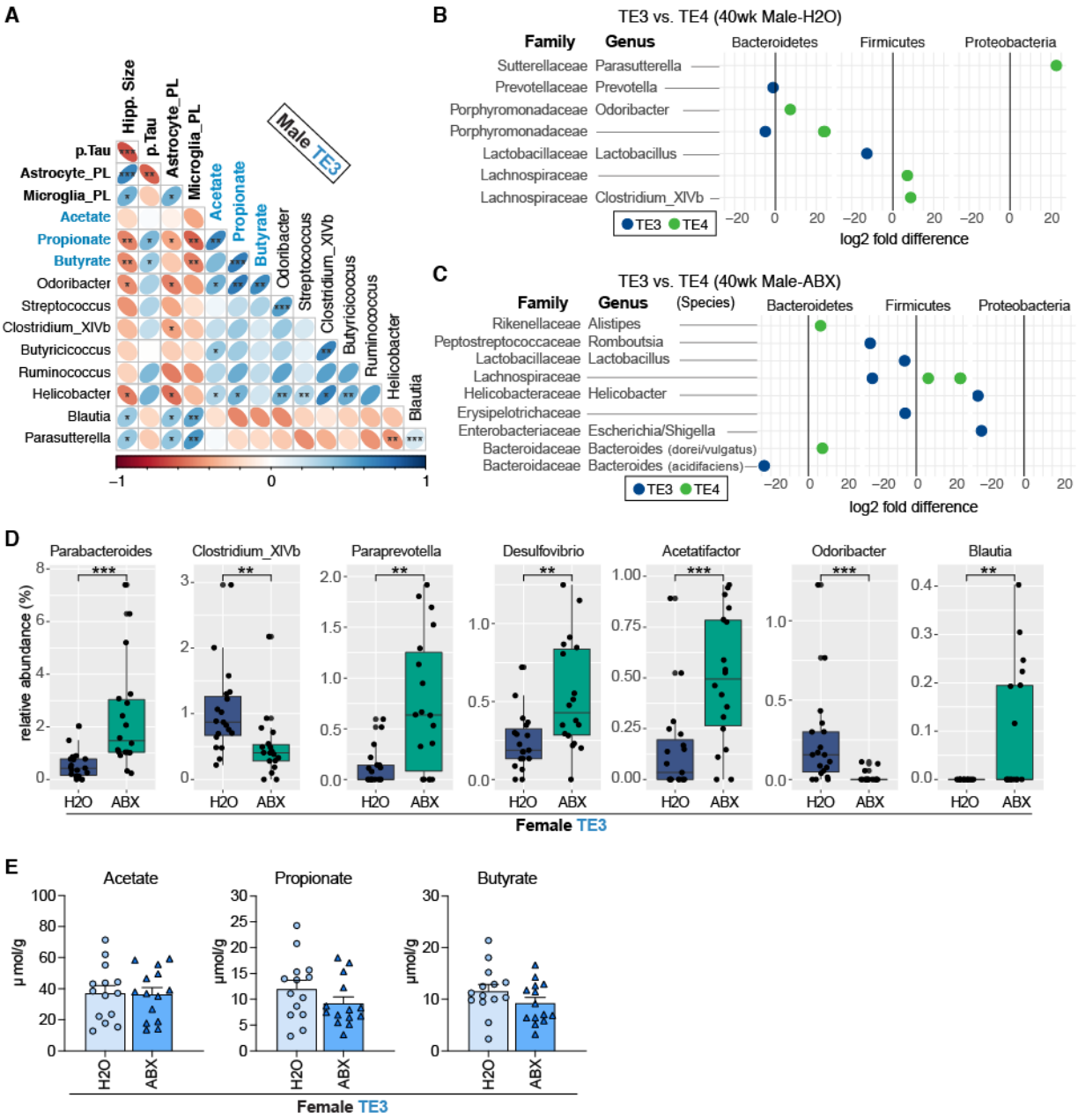

Fig. S13. Cecal levels of SCFAs in male TE3 associated with the interaction of GM and TN. Cecal levels of SCFAs in female TE3 mice are not significantly affected by ABX.
(**A**) Correlations between cecal levels of SCFAs (blue), the 8 genera identified as differentially abundant in male TE3-H2O, compared to TE3-ABX mice at 40 weeks of age, and biomarkers of tauopathy (bold) [hippocampus size (Hipp.S; smaller value reflecting greater neurodegeneration), coverage of AT8 staining, process length of astrocytes (astrocyte_PL), and process length of microglial cells (microglia_PL)] tested by Spearman's correlation. *, $p < 0.05$, **, $p < 0.01$, ***, $p < 0.001$. Related to **Fig. 5E**. Note that the correlation results between the 8 genera and biomarkers of tauopathy are different from **Fig. 5E** because the SCFA measurement was performed using a subset of animals selected based on the mean values of hippocampal volumes (n=14/group). (**B-C**) Comparison of relative abundance of taxa in TE3 versus TE4 mice at 40 weeks of age for

animals treated with H2O (B) or ABX (C). Log_2 fold differences are shown. (**D**) Comparison of relative abundance of taxa between treatments (H2O vs. ABX) in female 40-week-old TE3. Data are related to **Fig. 5B** and represented by log_2 fold differences. (**E**) Targeted GC-MS analysis of cecal short chain fatty acids in the ceca of 40-week-old female TE3 mice (n=14/group; t-test, p >0.05 for all metabolites).

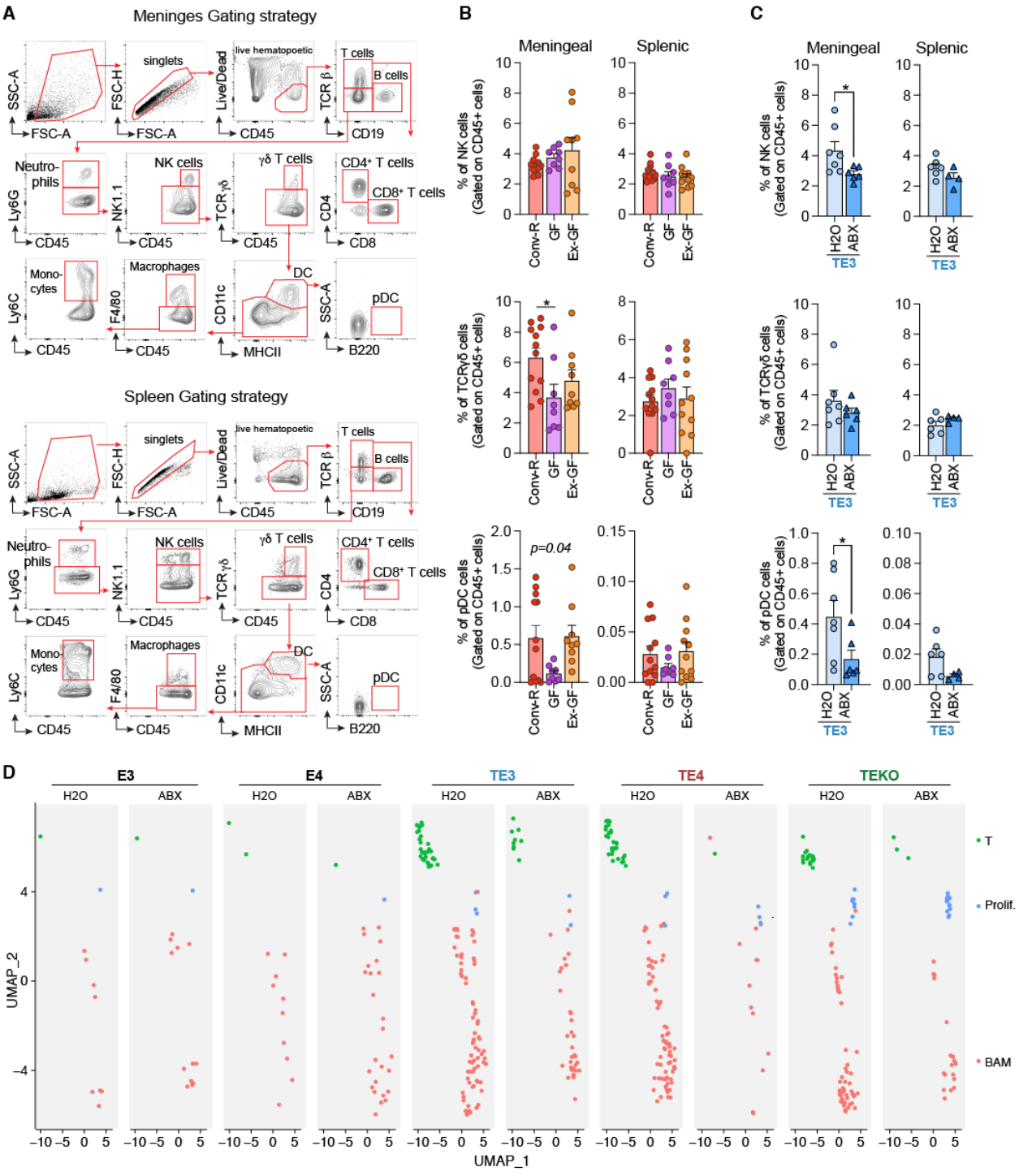

Fig. S14. Brain border innate and peripheral immune cells in mice with tau pathology are altered by germ free conditions and with ABX-induced gut microbiota perturbation.
(**A**) Flow cytometry plots showing the gating strategy used to identify different subsets of circulating immune cells in meninges (top) and spleen (bottom). (**B**) Frequency of meningeal NK cells (top), γδ T-cells (middle), pDC cells (bottom) in Conv-R, GF, and Ex-GF mice at 40 weeks of age. *n*=8-12/group, tested by one-way ANOVA and Tukey post-hoc test, *, $p < 0.05$. (**C**)

Frequency of meningeal NK (top), γδ T (middle), pDC (bottom) cells in male 40-week-old TE3 mice treated with H2O or ABX. n=6-7/group, tested by *t-test,* *, $p < 0.05$. (**D**) Additional snRNA-seq analysis using hippocampus tissue, related to **Fig. S8**, reveals that the populations of brain border and peripheral immune cells are reduced by ABX-induced gut microbiota perturbations. The UMAP plot shows the re-clustered population identified three distinguishable clusters, with corresponding cell types identified by using known cell markers. Abbreviations: T, T cells; Prolif., proliferating cells; BAM, border associated macrophage.

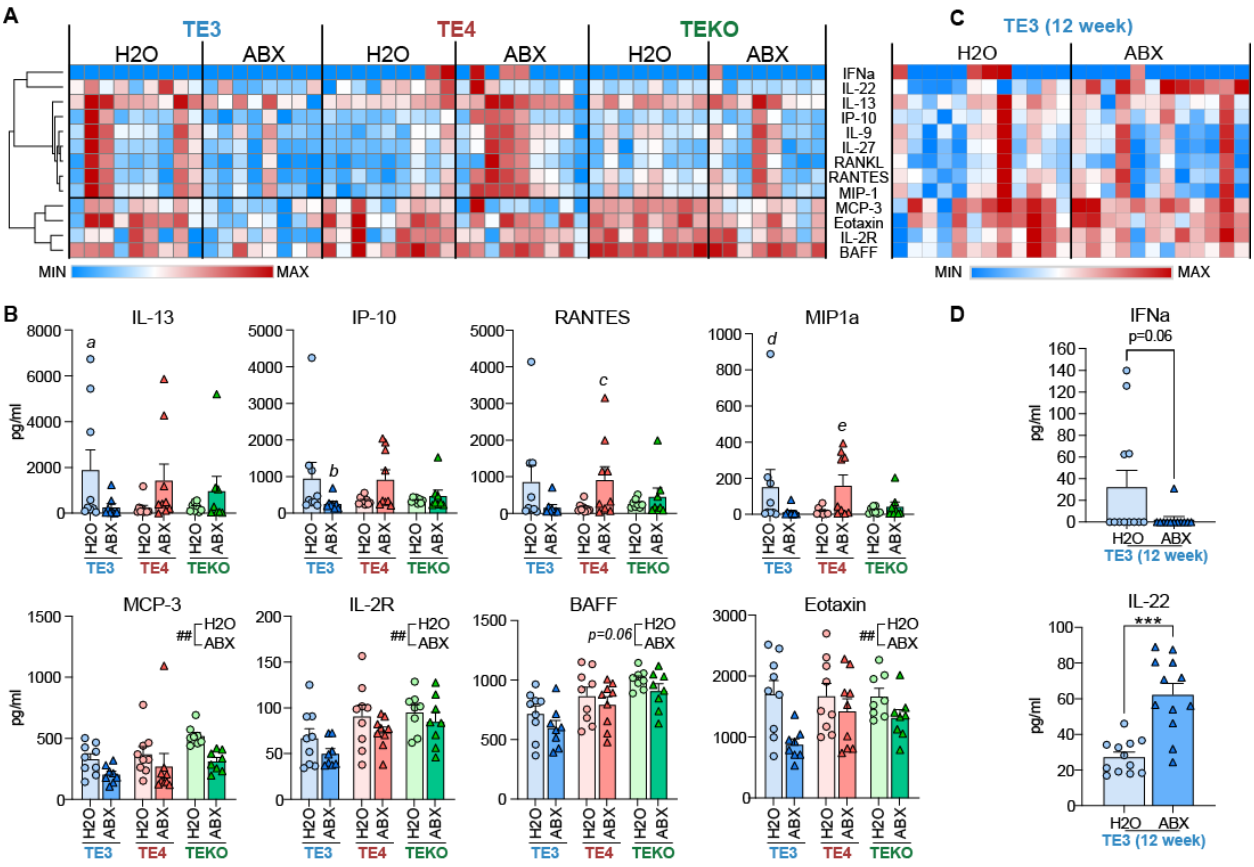

Fig. S15. ABX-induced gut microbiota perturbation is associated with the circulating inflammatory mediator profile.

(**A**) Heatmap and hierarchical clustering analysis of plasma cytokine and chemokine levels in 40-week-old male TE3, TE4, and TEKO treated with H2O or ABX. (**B**) Absolute levels of eight selected cytokine/chemokine in plasma samples obtained from male 40-week-old TE3, TE4, and TEKO mice treated with H2O or ABX (*n*=8-9/group). Statistical significance determined using two-way ANOVA., The main effects of treatments (H2O vs. ABX) were indicated as ##, $p < 0.01$. (**C**) Heatmap represents normalized plasma cytokine and chemokine levels in male 12-week-old TE3 mice treated with H2O or ABX. (**D**) Absolute levels of IFNα (top) IL-22 (bottom) in plasma samples obtained from male 12-week-old TE3 mice treated with H2O or ABX (*n*=12/group). Statistical significance determined using one-way ANOVA and Tukey post-hoc test for panel B and t-test for panel D. ***, $p < 0.001$. Statistically significant effects of treatments (H2O vs. ABX) are indicated as #, $p < 0.05$, ##, $p < 0.01$, ###, $p < 0.001$. In panel B, '*a*' indicates there was statistical significance for the interaction of genotype and treatment, but did not detect differences in *post-hoc*, '*b*' indicates that levels in TE3-ABX were significantly lower compared to TE3-H2O and TE4-ABX animals (p <0.05, with *LSD post-hoc*), '*c*' indicates that levels in TE4-ABX mice were significantly higher than TE3-ABX and TE4-H2O animals (p<0.05, *LSD post-hoc*), '*d*' indicates that values for TE3-H2O mice were significantly higher than the TE4-H2O treatment group, and *e* indicates that TE4-ABX was significantly higher than TE3-ABX and TE4-H2O groups. (see **Table S1** for full statistical results).

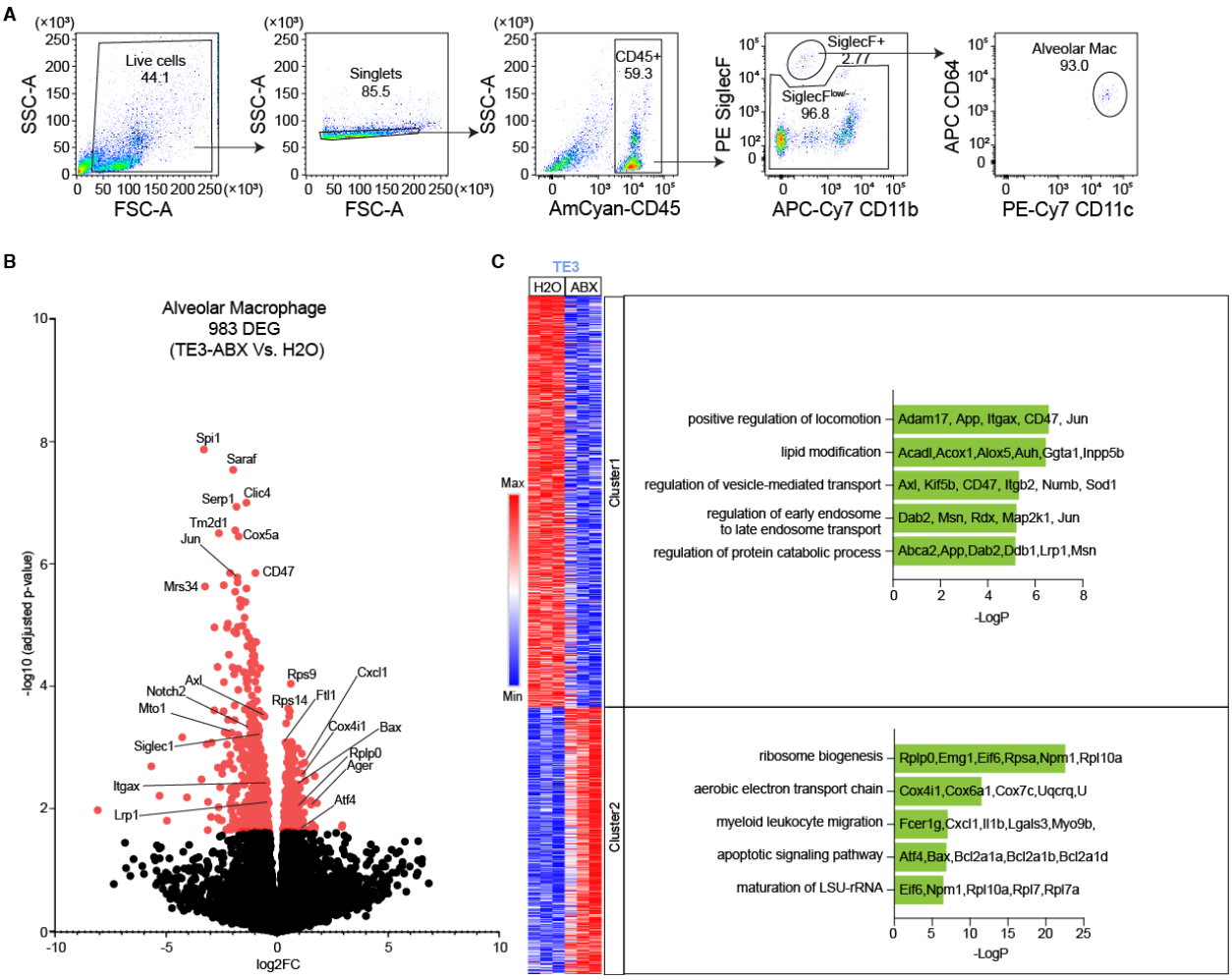

Fig. S16. ABX-induced gut microbiota perturbation altered peripheral macrophage transcriptomic signature.

(**A-C**) Summary of the RNA-seq results using isolated alveolar macrophages. (A) Flow cytometry plots showing the gating strategy used to identify alveolar macrophages, related to **Fig. S16-17**. (B) Volcano plots demonstrating the number of differentially expressed genes (DEG). Red points mark the genes with significantly increased/decreased expression (ABX versus H2O; adjusted $p<0.05$) in male 24-week-TE3 mice. (C) Cluster analysis of the DEGs in panel B. Each column represents one sample (n=3/group) and each row represents one differentially expressed gene. Boxes on the right side represent Gene Ontology (GO) Biological Process terms associated with Cluster 1 (top) and Cluster 2 (bottom) modules, ranked by *p*-value ($\log_{10}$P) with top 5 GO biological processes listed (See **Data S7** for a complete list of genes).

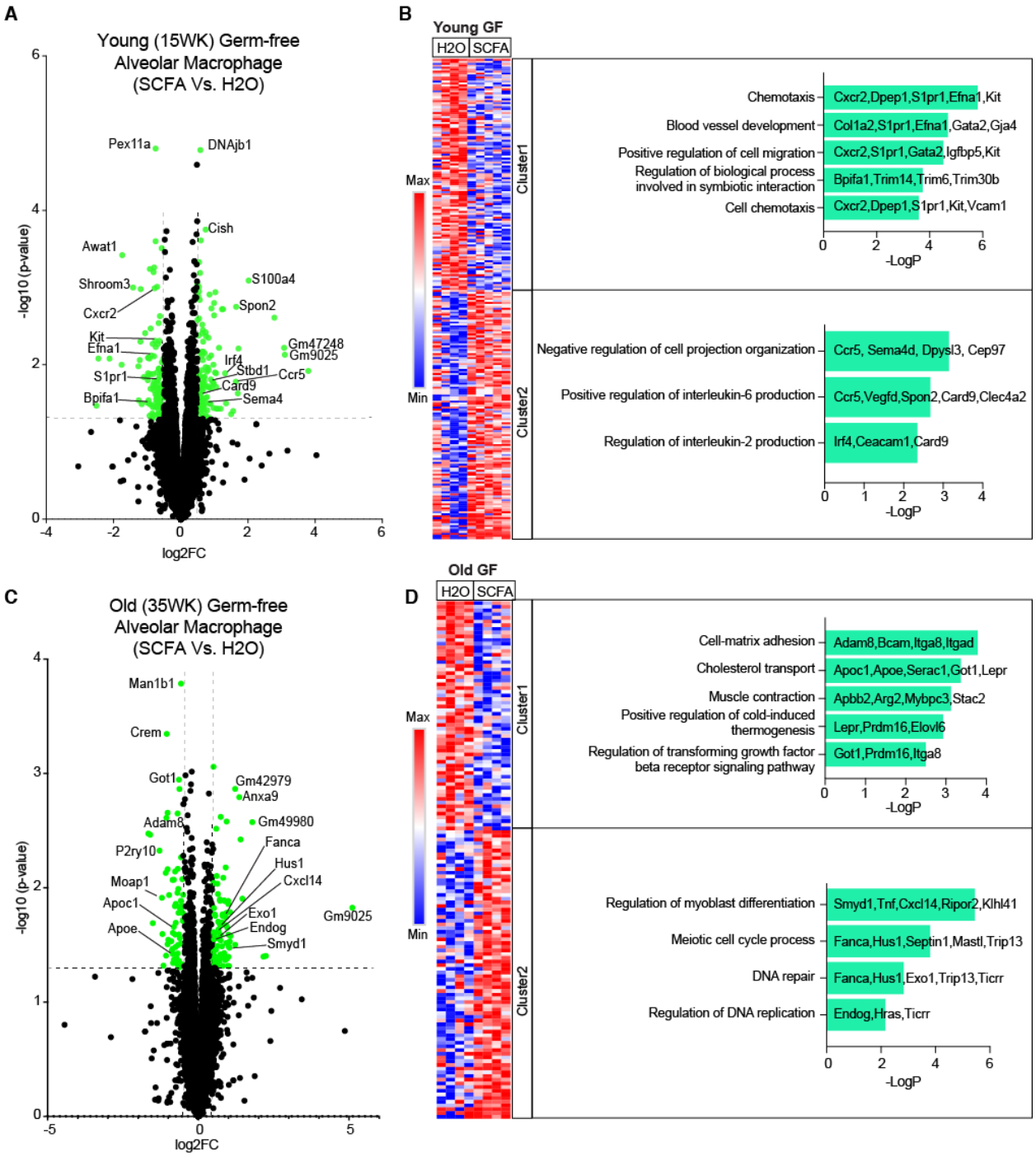

Fig. S17. SCFA supplementation alters peripheral macrophage transcriptomic signature in GF TE4 mice.

(**A-D**) Summary of the RNA-seq results using isolated alveolar macrophage samples from TE4 germ-free mice treated with either SCFA or H2O. *SCFAs* (all Sigma Aldrich, St. Louis, MO) were supplemented in the drinking water (sodium propionate, 25.9 mM; sodium butyrate, 40 mM; sodium acetate, 67.5 mM) and changed every 3 days for 5 weeks for 10-week-GF mice ('young' group) and 4 weeks for 31-week-GF mice ('old' group). **(A)** and **(C),** Volcano plots demonstrate the number of differentially expressed genes (DEG) in the alveolar macrophage samples. Green

points mark the genes with significantly increased/decreased expression based on unadjusted p-value (SCFA versus H2O; $p<0.05$) in male 15-week-GF mice (A) and 35-week-GF mice (C). Vertical lines represent the fold change cut-off (log2FC) at -0.5 and 0.5. (**B**) and (**D**), Cluster analysis of the DEGs in panels A (young) and C (old). Each column represents one sample (n=4-5/group), and each row represents one differentially expressed gene. Boxes on the right side represent Gene Ontology (GO) Biological Process terms associated with Cluster 1 (top) and Cluster 2 (bottom) modules, ranked by *p*-value ($\log_{10}$P) with top 5 GO biological processes listed (See **Data S8** for a complete list of genes).

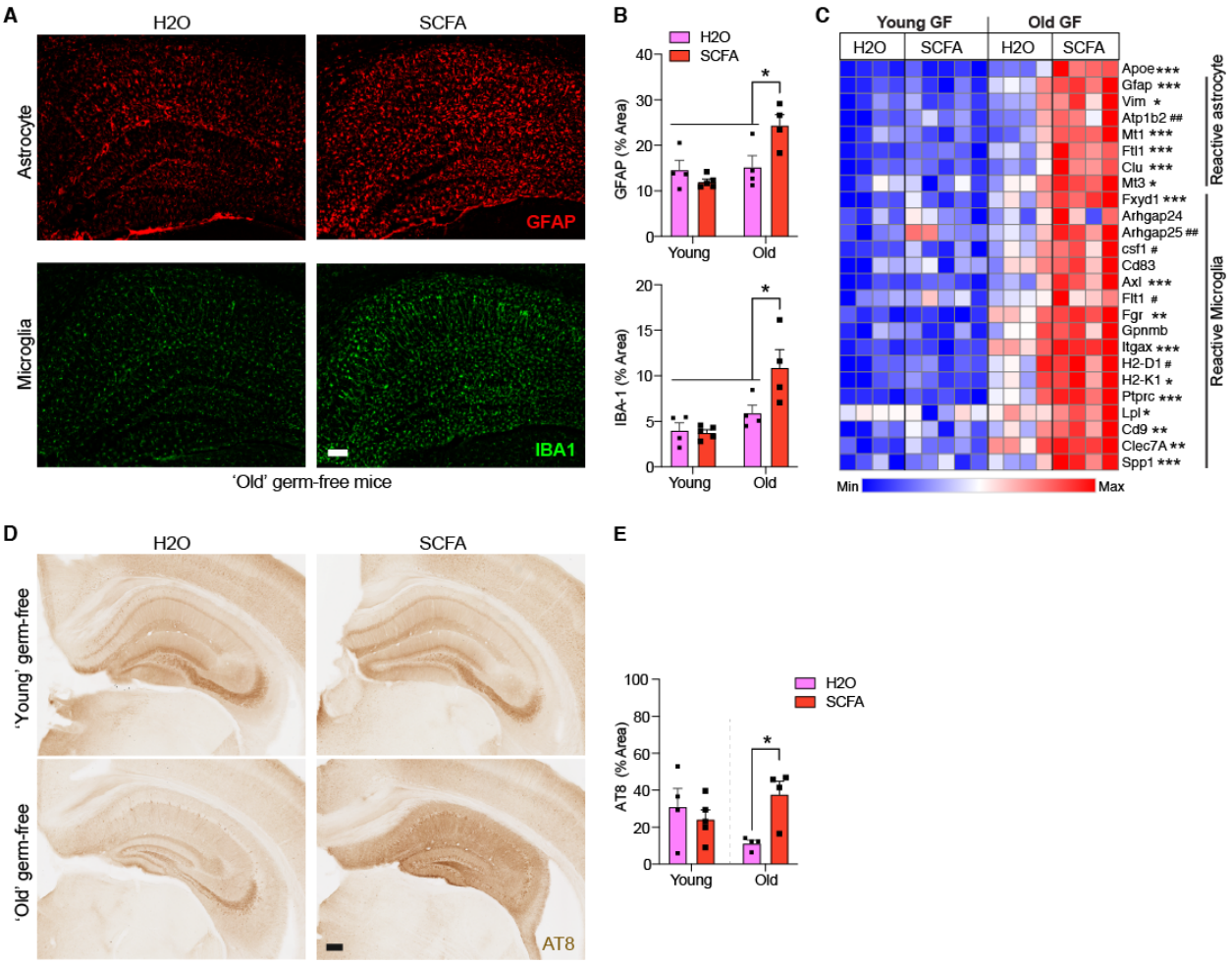

Fig. S18. SCFA supplementation promotes gliosis and tau pathology in GF TE4 mice (related to Fig. S17).

(**A**) Representative image of the hippocampus stained with either GFAP (top) or IBA1 (bottom), using brain samples collected from 'old' germ-free mice treated with H2O (left) or SCFA (right), scale bar, 100µm. (**B**) Percentage of the area covered by GFAP (top) and Iba-1 (bottom) in the hippocampus of 'young' (15-week-old) and 'old' (35-week-old) germ-free mice treated with either H2O or SCFA. (**C**) Heatmap represents normalized reactive glial gene expression measured by qPCR hippocampal tissues of 'young' and 'old' germ-free mice treated with either H2O or SCFA. The color scale represents normalized gene expression (RQ;$2^{-\Delta\Delta Ct}$) calibrating to the 'young-H2O' group. (**D**) Representative images of AT8 staining in the hippocampus from 'young' (top) and 'old' (bottom) germ-free mice treated with H2O (left) or SCFA (right), scale bar, 200µm. (**E**) Quantification of the percentage of area covered by AT8 staining of hippocampal sections. Data are presented as mean values ± SEM; Statistical significance determined by two-way ANOVA with Tukey's post-hoc test for panels B,C and t-test for panel E. *, $p < 0.05$. (see **Table S1** for full statistical results).